

Article

Lithium Extraction and Zeolite Synthesis via Mechanochemical Treatment of the Silicate Minerals Lepidolite, Spodumene, and Petalite

Tobias Necke ^{1,2,*} , Johannes Stein ¹, Hans-Joachim Kleebe ² and Benjamin Balke-Grünewald ¹

¹ Fraunhofer Research Institution for Materials Recycling and Resource Strategies IWKS, Aschaffener Straße 121, 63457 Hanau, Germany

² Institute for Applied Geosciences, Department of Geomaterial Science, Technical University of Darmstadt, Schnittspahnstraße 9, 64287 Darmstadt, Germany

* Correspondence: tobias.necke@iwks.fraunhofer.de

Abstract: Lithium is in high demand: this is driven by current trends in e-mobility and results in increased global production and record prices for lithium ores and compounds. Pegmatite ores, in addition to brines, remain of particular interest because of their higher lithium content and lower geopolitical risks. In this work, we investigated lithium extraction via the mechanochemical treatment of the three most common lithium minerals: lepidolite, spodumene, and petalite. Indeed, we determine that the petalite crystal structure was much more suitable due to its less dense packing and the formation of cleavage planes along lithium sites, resulting in substantial lithium extraction of 84.9% and almost complete conversion to hydrosodalite after 120 min of ball milling in alkaline media. Further processing of the leach liquor includes desilication, the precipitation of lithium phosphate, and the conversion and crystallization of pure LiOH·H₂O. Special attention was paid to a holistic approach entailing the generation of by-products, each of which has a specific intended application. The leaching residues were investigated by powder X-ray diffraction, Fourier transform infrared spectroscopy, N₂ adsorption/desorption, and scanning electron microscopy. Moreover, hydrosodalite was found to have a high potential as an adsorbent for heavy metal ions which were studied separately using aqueous solutions containing Cu²⁺, Ni²⁺, Pb²⁺, and Zn²⁺.

Keywords: lithium; mechanochemistry; hydrosodalite; petalite; mineral processing



Citation: Necke, T.; Stein, J.; Kleebe, H.-J.; Balke-Grünewald, B. Lithium Extraction and Zeolite Synthesis via Mechanochemical Treatment of the Silicate Minerals Lepidolite, Spodumene, and Petalite. *Minerals* **2023**, *13*, 1030. <https://doi.org/10.3390/min13081030>

Academic Editors: Zhao Li, Huimin Hu, Xuewei Li and Qiwu Zhang

Received: 30 June 2023

Revised: 25 July 2023

Accepted: 30 July 2023

Published: 31 July 2023



Copyright: © 2023 by the authors. Licensee MDPI, Basel, Switzerland. This article is an open access article distributed under the terms and conditions of the Creative Commons Attribution (CC BY) license (<https://creativecommons.org/licenses/by/4.0/>).

1. Introduction

In recent years, lithium has become a strategic element, especially in the context of the transition from combustion engines to electromobility, as it combines the highest electrochemical potential of all alkali metals with its remarkably low atomic weight [1–3]. Currently, about 80% of the world's lithium demand is used for battery production while more traditional lithium applications such as ceramics and glasses (7%), lubricating greases (4%), continuous casting powders (2%), air treatment (1%), or pharmaceutical applications (1%) play only a minor role [4]. However, due to current developments in electromobility, lithium is in high demand, leading to an increase in global production of 21% from 107,000 tons (2021) to 130,000 tons (2022) and record prices for spodumene ore (6% lithium oxide content; 5800 US\$/t) and for the most common compounds Li₂CO₃ (67,000 US\$/t) and LiOH (78,000 US\$/t) in November 2022 [4]. Since the steadily increasing demand has not been compensated by efficient recycling of end-of-life products, the mining of primary resources is still mandatory to enable large-scale battery production. Economically viable deposits are only found in specific geological environments such as continental brines or granitic pegmatites, although lithium is quite common from a geological perspective; however, it is at low concentrations in igneous rocks of the Earth's crust [5–7]. In terms of the general size and total estimated resources, pegmatite deposits are often much smaller

than brine deposits but they remain of particular interest due to their higher lithium content and their broader geographic distribution, which consequently poses lower geopolitical risks [8,9]. In addition, the extraction of lithium compounds from mineral ores is a much faster process than processing from brine as no time-consuming evaporation is required, which makes it suitable for responding flexibly to market fluctuations [8,10].

However, in addition to these advantages, the processing of pegmatite ores including the minerals lepidolite $K(Li_2Al)(Si_4O_{10})(F,OH)_2$ to $K(Li_{1.5}Al_{1.5})(AlSi_3O_{10})(F,OH)_2$, spodumene ($LiAlSi_2O_6$), and petalite ($LiAlSi_4O_{10}$) presents some challenges, such as their low reactivity resulting in poor leachability [9,11,12]. In order to convert these minerals into a more reactive form, namely that in which the lithium atoms/ions are more accessible to the extraction reagent, energy-intensive high-temperature treatments such as calcination and sulfuric acid roasting are mandatory in most established processing routes [3,9,13]. During calcination at about 1000 °C, the monoclinic minerals lepidolite, α -spodumene, and petalite transform into tetragonal β -spodumene (space group $P4_32_12$) which has a lower density, a more open structure, and is therefore much more susceptible to leaching especially when compared to α -spodumene [7,13,14].

In addition to conventional heating, microwave heating and mechanical activation are also being considered as alternative pretreatment methods [12]. Especially, the use of microwave-assisted heating enables faster and more energy-efficient production of β -spodumene but requires special furnaces including silicon carbide crucibles for rapid heat transfer [12,15]. In particular, it has been shown that the mechanical activation of spodumene, which includes ball milling in air and aqueous media, can lead to an increase in specific surface area, a reduction in particle and crystallite sizes, and the formation of amorphous phases, which are generally favorable conditions for achieving high leaching rates [12,16,17]. Moreover, similar experiments on mechanical activation were performed on lepidolite specimens which confirmed the results obtained for spodumene [11,18].

The industrial state of the art of processing has so far focused only on the comparatively low but economically important lithium content of these silicates while the main constituents Al and Si have been neglected, resulting in 8 to 10 tons of leaching residues per ton of Li_2CO_3 during sulfuric acid leaching of spodumene [9,19]. These findings have encouraged authors to explore approaches that utilize the entire inventory of lithium minerals such as lepidolite [20], spodumene [21], or petalite [22] by alkaline leaching in high pressure autoclaves. It is noteworthy that these processes are carried out without thermal phase transformation under strongly alkaline conditions, usually hydrothermally in an autoclave, to decompose the silicates and enrich lithium in the solution [22–24]. In addition, Lv et al. [20] and Xing et al. [21] employed the alkaline treatment for the parallel synthesis of zeolites, while Qui et al. [25] produced $KAlSiO_4$ as a zeolite precursor as value-added by-products through the use of Al and Si derived from lithium silicate minerals. Especially, sodium zeolites such as hydrosodalites with the general formula $Na_{6+x}[Al_6Si_6O_{24}](OH)_x \cdot nH_2O$ synthesized along alkaline routes are known for their special properties in molecular sieving or selective adsorption, rendering them as potential materials for the removal of hazardous heavy metal ions in aqueous media or membrane materials [26–28].

In a previous study, the authors already combined the approaches of mechanical activation and alkaline decomposition by performing mechanochemical experiments on lithium extraction and zeolite synthesis from end-of-life $Li_2O-Al_2O_3-SiO_2$ glass-ceramics [29]. There, the possibility of achieving high extraction efficiency with the combined ball milling approach under rather mild conditions based on the use of NaOH and without external temperature or pressure supply, which is common in autoclaves, was demonstrated [29]. In the context of ongoing studies on lithium extraction and zeolite synthesis, this work investigated the transferability of the previous extraction route to the three most common lithium silicate minerals: lepidolite, spodumene, and petalite.

2. Materials and Methods

Samples in this study include spodumene from the Sahatany pegmatite field in the Vakinankaratra region of central Madagascar (acquired from MIKON Mineralienkontor GmbH, Gleichen, Germany), lepidolite from the Bikita pegmatite near Masvingo, Zimbabwe, and petalite from the Luolamäki pegmatite close to Somero, Finland (acquired from Rockhunter Handels UG, Waldalgesheim, Germany), which were investigated with respect to lithium extraction and zeolite synthesis.

Pretreatment of the samples became necessary to obtain a fine and homogeneous powder for the leaching experiments in which the lithium-bearing silicates were crushed with a jaw crusher (Pulverisette 1, Fritsch, Idar-Oberstein, Germany), comminuted to a fine powder with a disk mill (Pulverisette 9, Fritsch, Germany), and then sieved to a particle size of less than 500 μm . Moreover, samples were additionally hand-picked after jaw crushing to remove natural accompanying phases and altered sample parts as both could influence further analyses and experiments.

Experimental procedures used during the mechanochemical investigations are described in detail in one of our earlier publications on the recycling of end-of-life glass ceramics [29]. In this work, the previous findings were extended to the three economically most important naturally occurring lithium mineral sources: spodumene, lepidolite, and petalite. During the mechanochemical experiments, the sample powders were milled in a sodium hydroxide solution of varying concentrations (NaOH; Carl Roth, Karlsruhe, Germany, $\geq 99\%$) using a planetary ball mill (Pulverisette 6, Fritsch, Germany) equipped with a 250 mL vessel and grinding balls, both of which were made of stainless steel. In the scope of this fundamental study, only the experimental parameters, namely the milling time and NaOH concentration, were varied within well-known ranges to investigate their influence on lithium extraction and zeolite formation, while other parameters such as the rotation speed, ball-to-powder ratio (BPR), liquid-to-solid ratio (LSR), sample amount, and ball size were kept constant at 600 rpm, 50 g/g, 10:1 mL/g, 10 g, and 10 mm, respectively, throughout the study. After alkaline treatment in the ball mill, the resulting suspension was separated into a lithium-rich liquid and solid sediment. In addition, the solid fraction was washed with deionized water to remove adhering NaOH, dried at 85 °C for 48 h, and finally homogenized using a mortar and pestle.

Desilication of the caustic solution after extraction became necessary as an intermediate step prior to lithium precipitation. The approach of Xing et al. [30] was chosen here to remove aluminum and silicon by adding calcium oxide at 95 °C. Therefore, defined amounts of calcium oxide (CaO; Carl Roth, $\geq 96\%$) were added to the preheated solution in the molar ratios of 0.6, 0.8, 1.0, and 1.4 according to the CaO/SiO₂ ratio. After a total time of 120 min, the solid residue was separated from the lithium rich solution, washed, dried at 85 °C for 48 h, and then calcined at 900 °C for 30 min in a muffle furnace.

Precipitation and conversion of lithium compounds were achieved following the procedure of Mulwanda et al. [23]. During precipitation, small amounts of phosphoric acid (H₃PO₄, 85%, Carl Roth, analytical grade) were added through a glass cannula to the preheated caustic solution in a round bottom flask to produce lithium phosphate (Li₃PO₄). The amount used here corresponded to the molar ratios of 1.0:3.0; 1.2:3.0; 1.4:3.0; 1.6:3.0; and 1.8:3.0 of phosphorus to lithium. After stirring for an additional 60 min, the solid product was separated, washed several times with deionized water, and finally dried at 85 °C for 48 h. For the conversion into lithium hydroxide (LiOH·H₂O), 1.65 g Li₃PO₄ was mixed with 50 mL deionized water in a reflux vessel with the addition of calcium hydroxide (Ca(OH)₂, Sigma Aldrich, Burlington, MA, United States, 99%) in a 1.8-fold molar excess, heated to a temperature of 60 °C, and held for 120 min. After the liquid–solid separation, crystallization of the dissolved LiOH·H₂O was initiated by evaporating the solution under an argon atmosphere which is required to avoid the interaction with carbon dioxide from the air that would lead to the formation of lithium carbonate.

Adsorption experiments were conducted with synthetic wastewater samples containing two valent heavy metal ions Pb²⁺, Cu²⁺, Zn²⁺, or Ni²⁺ to investigate the adsorption

characteristics of the zeolite by-products. For this purpose, single metal solutions of analytical grade (Titrisol, Merck, Darmstadt, Germany) were diluted to a concentration of 100 mg/L. In this study, the metal removal efficiencies were monitored for various adsorbent dosages ranging from 1 g/L to 15 g/L by adding 50, 100, 150, 200, 300, 400, 500, 600, and 750 mg of zeolite to 50 mL of wastewater. To ensure proper adsorption conditions, the suspensions were shaken at room temperature (20 ± 1 °C) in an overhead shaker at 10 rpm for 120 min followed by liquid–solid separation by centrifugation.

Analytical methods include inductively coupled plasma optical emission spectrometry (ICP-OES; Optima 8300 instrument, PerkinElmer, Waltham, MA, USA) which was used to evaluate the extraction, desilication, precipitation, and adsorption experiments. Prior to analysis, solid silicate samples required fusion with sodium peroxide (Na_2O_2 ; Merck, $\geq 95\%$) in a zirconium metal crucible (HRT Fusion, Seevetal, Germany) and digestion with hydrochloric acid (HCl; Merck, analytical grade). For the determination of the loss on ignition (LOI) at 1050 °C, an STA 449 F3 Jupiter thermo-gravimetric analyzer (Netzsch, Selb, Germany) was selected. Powder X-ray diffraction (PXRD) using an X-ray diffractometer (Empyrean, Malvern Panalytical, Malvern, UK) equipped with a cobalt source, operating in Bragg–Brentano geometry at 40 mA and 40 kV, was utilized for phase analysis of solid samples. During measurement, diffraction patterns were recorded for the 2θ range of 10 to 75° using a scan speed of 0.006°/s and a step size of 0.013° and analyzed by the software HighScore Plus (Malvern Panalytical, UK) including the inorganic crystal structure database (ICSD; FIZ Karlsruhe, Karlsruhe, Germany). Fourier transform infrared (FT-IR) examinations were conducted on a Nicolet iS50 spectrometer (Thermo-Fisher Scientific, Waltham, MA, USA) across the wavelength range from 4000 to 400 cm^{-1} using KBr pellets (Carl Roth, analytical grade) to investigate changes in molecular bonding. Therefore, 32 scans were performed for each sample with a resolution of 4 cm^{-1} . In addition, the Brunauer–Emmet–Teller (BET) method was applied to determine the specific surface areas of the zeolite samples by measuring N_2 adsorption/desorption at -196 °C on a 3Flex adsorption device (Micromeritics, Norcross, GA, USA). Therefore, the specimens are preconditioned by outgassing using a Smart VacPrep (Micromeritics, USA) preparation device at 200 °C for 720 min. Moreover, the morphological features and microstructure of the synthesized zeolite samples were checked by scanning electron microscopy (SEM) using a Merlin SEM (Zeiss, Jena, Germany) while information on the chemical composition was obtained by energy-dispersive X-ray spectroscopy (EDS) using an XMAX 80 detector (Oxford, UK).

The extraction rate for lithium R_{Li} [%] was calculated based on ICP-OES results according to Equation (1) where C_o [g/L] is the mass concentration of metal ions in the leachate, V_o [L] is the leachate volume, m [g] is the sample mass, and $w\%$ [g/g] is the metal mass fraction of lithium in the source materials.

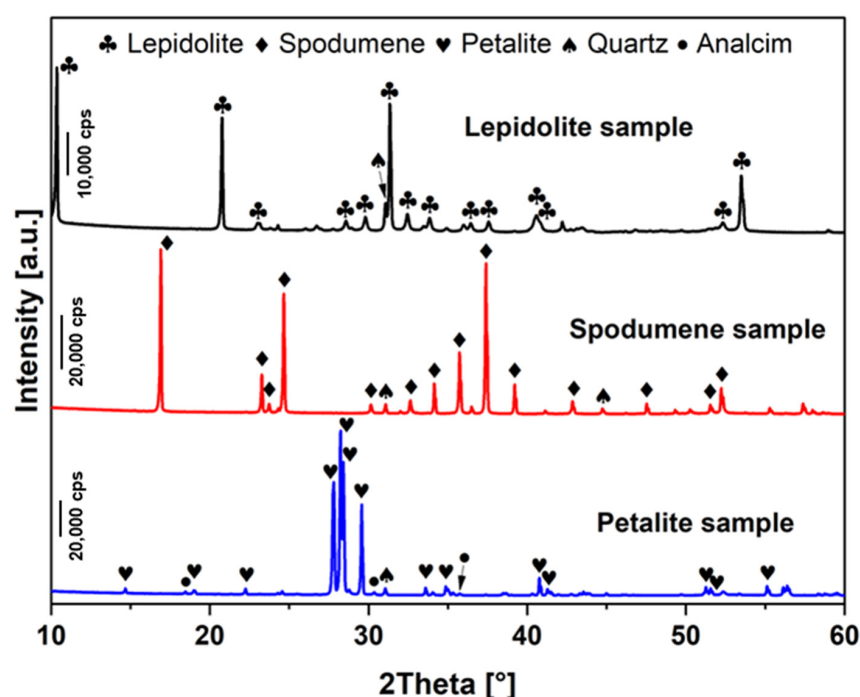
$$R_{Li} = (C_o \times V_o) / (m \times w\%) \times 100 \quad (1)$$

Characterization of the feed materials involves ICP-OES measurements (shown in Table 1) indicating Li_2O contents of 5.6 wt% (lepidolite), 7.3 wt% (spodumene), and 5.2 wt% (petalite) besides the main element's silicon and aluminum. Moreover, the lepidolite samples additionally show K_2O and also Rb_2O as main constituents, while the LOI value of 3.0% indicates the presence of volatile compounds such as OH and F.

In addition, PXRD measurements (Figure 1) on the source materials yielded rather pure mineral samples of lepidolite (PDF#98-003-0784), spodumene (PDF#98-028-0109), and petalite (PDF#98-010-0348) with only minor natural cogenetic phases such as α -quartz (PDF# 98-020-1354). Furthermore, traces of analcime (PDF#98-004-0451) were only detected in petalite samples as a natural impurity which is consistent with data in the literature [31].

Table 1. Chemical composition of the feed materials based on ICP-OES measurements and transferred into oxide values.

[wt%]	Lepidolite	Spodumene	Petalite
Al ₂ O ₃	23.8	27.3	16.2
CaO	n.n.	n.n.	0.1
Fe ₂ O ₃	0.1	0.4	0.1
K ₂ O	12.3	0.2	0.4
Li ₂ O	5.6	7.3	5.2
MnO	0.7	0.1	n.n.
Rb ₂ O	1.7	n.n.	n.n.
SiO ₂	52.4	64.5	71.1
LOI	3.0	0.4	0.5

**Figure 1.** PXRD patterns of the investigated feed materials lepidolite, spodumene, and petalite.

3. Results

Mechanochemical treatment combining ball milling of lithium silicates with alkaline leaching were investigated since it is known from the literature that alkaline solutions are able to extract lithium from aluminosilicate minerals such as lepidolite [20,23], spodumene [21,24], and petalite [22] by decomposing their silicate structure. Moreover, they are widely used for alkaline activation in the synthesis of zeolites [32]. Therefore, we studied the combined approach in terms of lithium extraction and zeolite synthesis. In order to study whether the promising experimental parameters of our previous work on Li₂O-Al₂O₃-SiO₂ glass-ceramics are transferable to naturally occurring lithium silicates, several ball milling experiments were performed. For this purpose, the NaOH concentration was varied between 7 and 9 mol/L at different reaction times of 30, 60, and 120 min to study their influence on lithium extraction and zeolite formation while the rotation speed, ball-to-powder ratio, liquid-to-solid ratio, sample amount, and ball size were kept constant. The overall results of the extraction experiments are summarized in Figure 2 where a lithium extraction rate for lithium as a function of reaction time was calculated for each experiment based on ICP-OES measurements according to Equation (1). As can clearly be seen, there are significant differences in lithium extraction between the three minerals investigated. When lepidolite was used as a lithium source, the yield was gen-

erally the lowest, reaching a maximum of 18.2% at 120 min using 7 mol/L NaOH while a slightly higher yield of 28.4% was obtained when spodumene was processed with the same parameters.

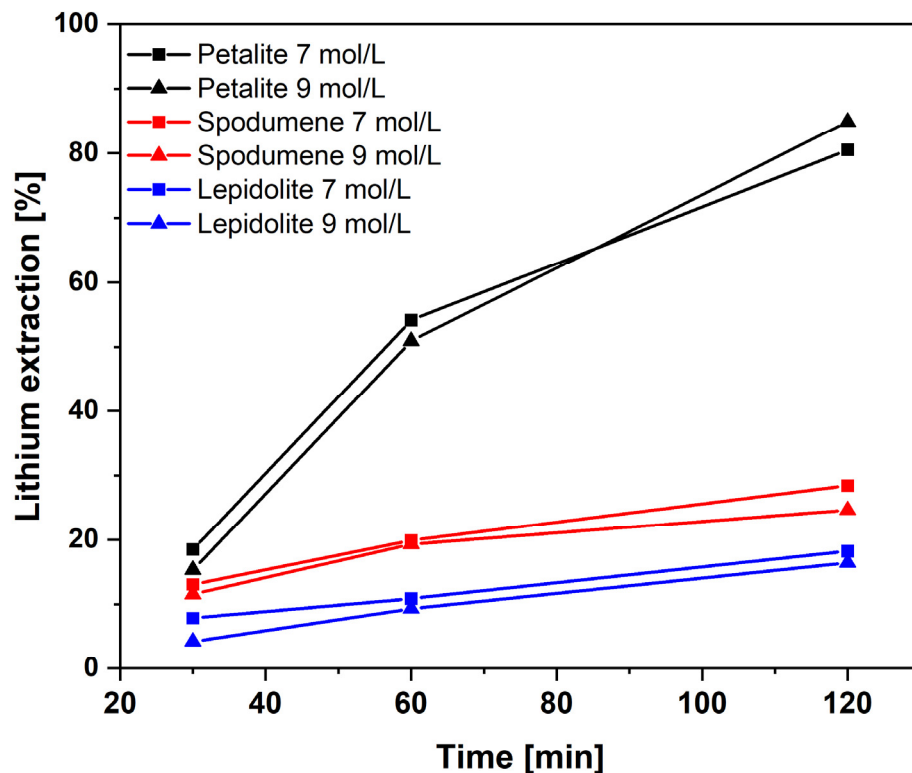


Figure 2. Recovery rates for lithium extracted from the minerals petalite, lepidolite, and spodumene at different reaction times using 7 or 9 molar concentrations of sodium hydroxide solution.

Surprisingly, the experiments with petalite yielded a remarkably higher extraction efficiency than the corresponding trials with lepidolite or spodumene. It should be noted that at a time of 30 min, the yield was only slightly higher, while at 60 and 120 min significantly higher values of 54.1 and 84.9% could be achieved. For the influence of the sodium hydroxide concentration on extraction, there is no clear trend to report as there are only minor differences between the 7 and 9 mol/L experiments.

XRD measurements on leaching residues were chosen to evaluate the effects of mechanochemical treatment on the degradation of the lithium-containing phases in addition to ICP-OES analysis of the liquid samples. In the following (see Figures 3–5), only the diffraction patterns of experiments at 7 mol/L are described since there were only subtle variations between the two investigated sodium hydroxide concentrations.

The results for the lepidolite samples shown in Figure 3 indicate no significant changes in phase composition or the formation of new phases during ball milling experiments conducted for up to 120 min. Furthermore, similar results were obtained for spodumene samples milled for only 30 or 60 min (see Figure 4), with no significant change in the diffraction peaks monitored. In contrast, the mechanochemical treatment for 120 min led to less intense diffraction peaks of spodumene and the formation of hydrosodalite (SOD, PDF#98-003-6050), both of which can be interpreted as the first signs of a breakdown of the initial phase. Investigations on petalite samples (see Figure 5) showed the appearance of hydrosodalite diffraction peaks after 60 min of milling, which became significantly more intense as the reaction time increased to 120 min in parallel with petalite peaks that became considerably weaker. Accordingly, these results indicate progressive decomposition, reconstruction, and transformation of the parent petalite phase into a hydrosodalite zeolite while ball milling in alkaline media. These results are consistent with our previous work

using glass ceramics as a lithium source, where SOD was the dominant zeolite phase along with zeolite N (LTN) using 7 or 9 mol/L NaOH [29]. On closer inspection, minor remnants of petalite were still present at 120 min, indicating that phase transformation was not yet completed. In addition, traces of quartz and analcime occurred in several diffraction patterns which can be attributed to inhomogeneities in the natural source material.

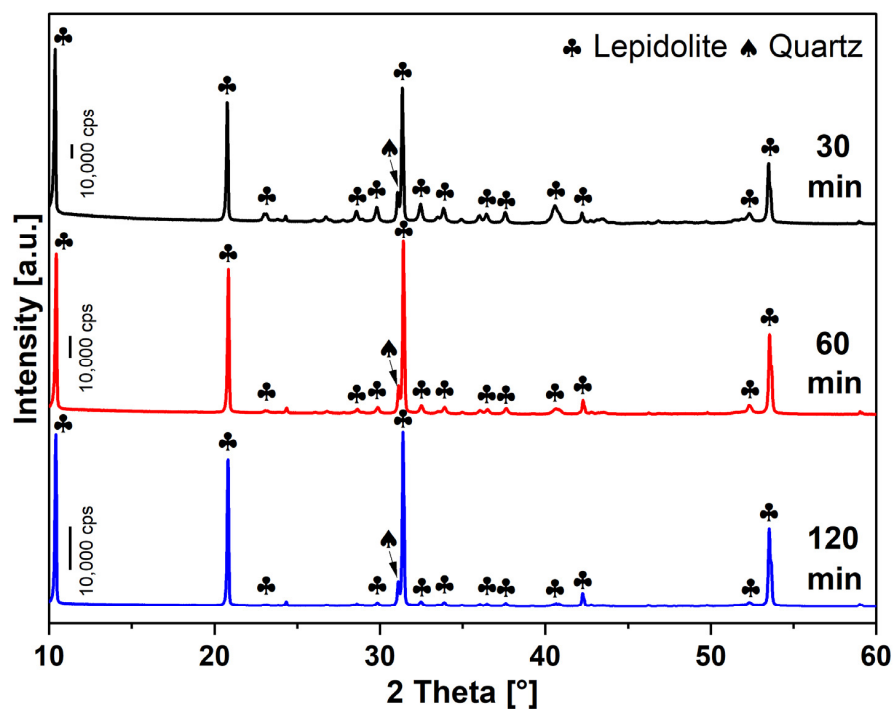


Figure 3. PXRD patterns of the leaching residues after mechanochemical treatment of lepidolite using 7 mol/L NaOH solution at different reaction times.

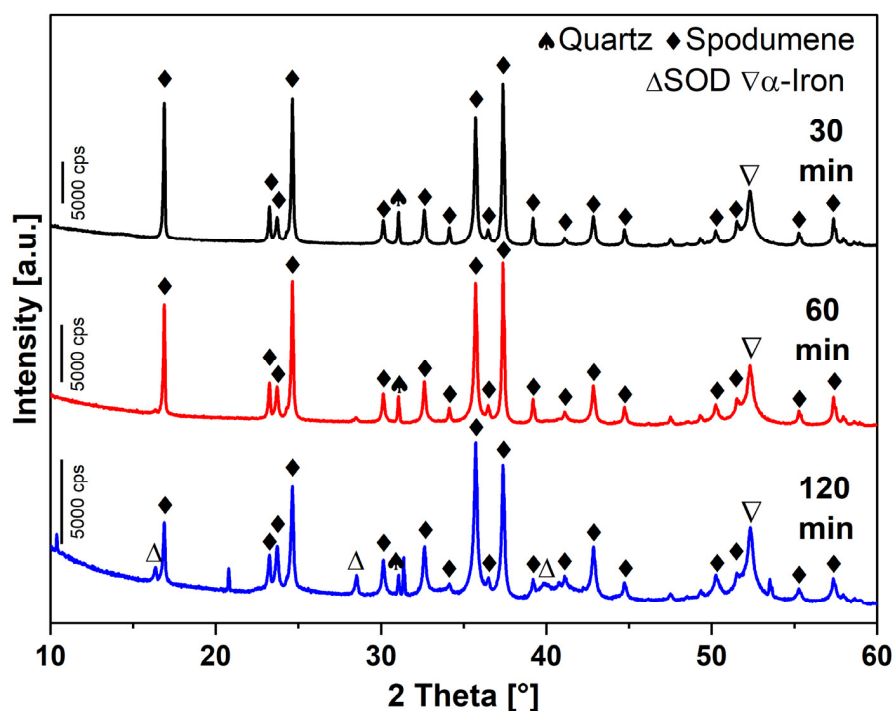


Figure 4. PXRD patterns of the leaching residues after mechanochemical treatment of spodumene using 7 mol/L NaOH solution at different reaction times.

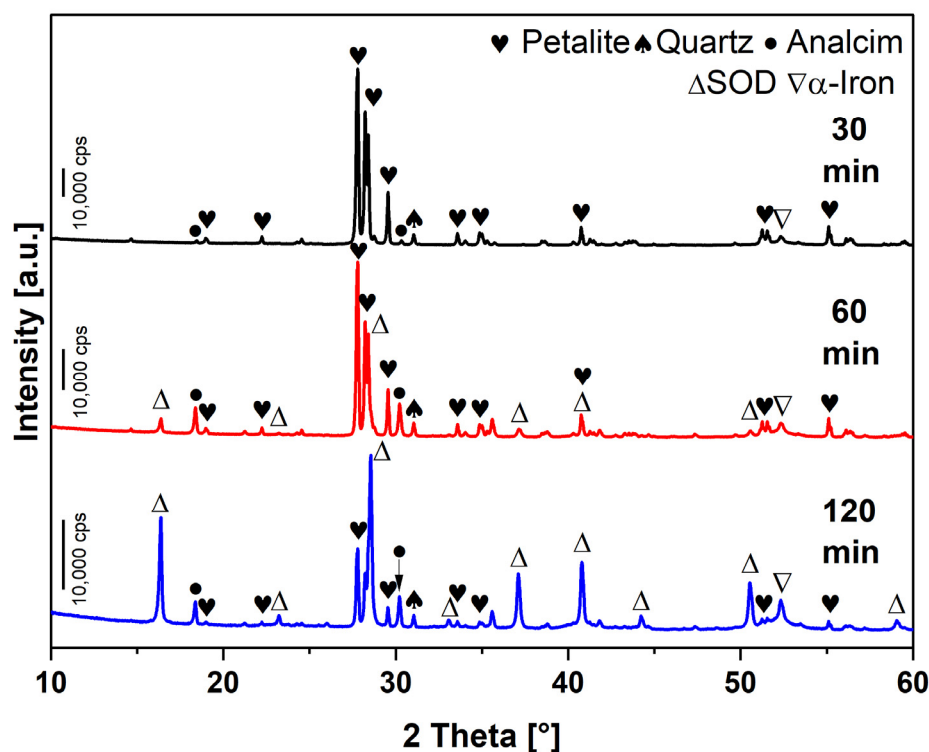


Figure 5. PXRD patterns of the leaching residues after mechanochemical treatment of petalite using 7 mol/L NaOH solution at different reaction times.

FTIR spectroscopy was selected to determine changes in molecular bonding of aluminum and silicon during alkaline treatment with 7 mol/L NaOH solution at constant milling parameters for different times. The resulting spectra shown in Figure 6 indicate a reorganization in molecular bonding after mechanochemical treatment. The first changes became visible in the range of 1000 cm^{-1} in the 60 min sample while the characteristic stretching vibrations of petalite at 1223 , 1084 , and 1022 cm^{-1} disappeared completely after 120 min, indicating a structural change. In this sample, SOD could be clearly identified by its typical Si–O–T (T = Al, Si) stretching and bending vibrations at 993 , 734 , 706 , and 663 cm^{-1} in addition to the bending of oxygen bridges at 465 and 436 cm^{-1} . In general, FTIR spectra obtained for petalite and hydrosodalite agree well with data in the literature and support the PXRD measurements, both of which indicate the decomposition of petalite and transformation into sodalite with progressive reaction times.

The overall result of the alkaline mechanochemical treatment indicates Equation (2) in which petalite is converted to basic hydrosodalite while lithium and fractions of silica (represented by $\text{Si}(\text{OH})_4$) are leached into the liquor.



SEM including EDS analysis were selected to examine the microstructure of the leaching residues of petalite samples after 120 min of ball milling and to determine the size, morphology, distribution, and local chemistry of the crystallites. As depicted in Figure 7, the sample consists mainly of intergrown isometric crystals with a size of about 200 to 800 nm, showing a pronounced dodecahedral habit and are mainly composed of Na, Al, Si, and O (SEM-EDS) which are all known to be characteristic features of hydrosodalites. In particular, the occurrence of pristine crystals with euhedral habits and sharp edges was unexpected for a ball-milled sample indicating undisturbed crystallization during the process. Remnants of unreacted petalite in the form of tiny cleavage lamellae and platelet-shaped iron-containing fragments were also detected by SEM-EDS analysis, which is in accordance with the PXRD measurements. Minor amounts of iron in the residues are

attributed to a slight abrasion during milling which is most pronounced in the spodumene samples (see Figure 4) as a result of its higher hardness. However, this had no effect on the overall extraction process since iron is insoluble at high pH values.

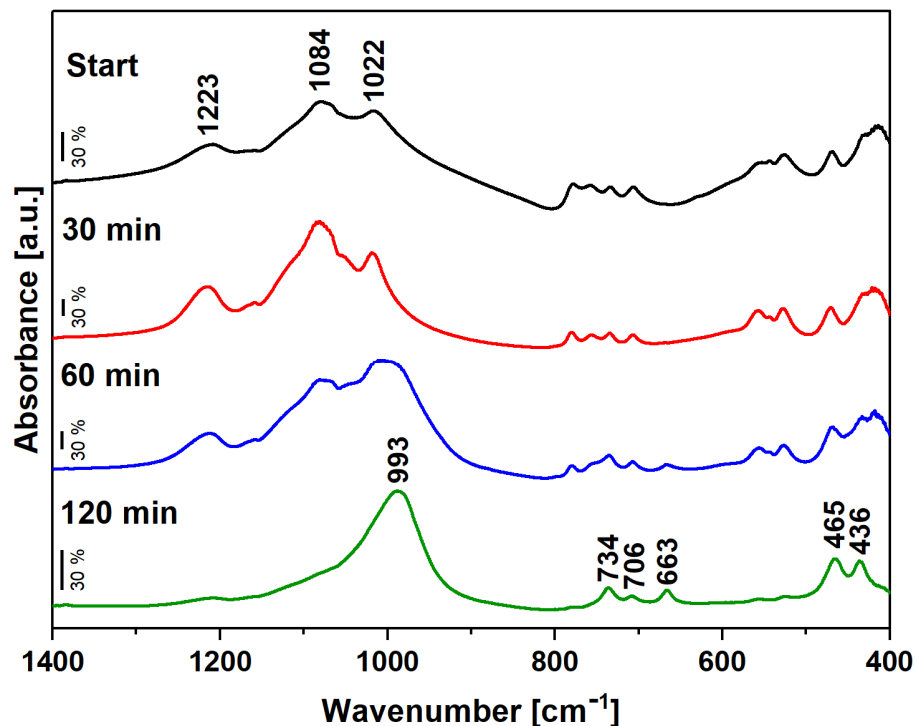


Figure 6. FTIR spectra of petalite source material and leaching residues after mechanochemical treatment using 7 mol/L NaOH solution at different reaction times.

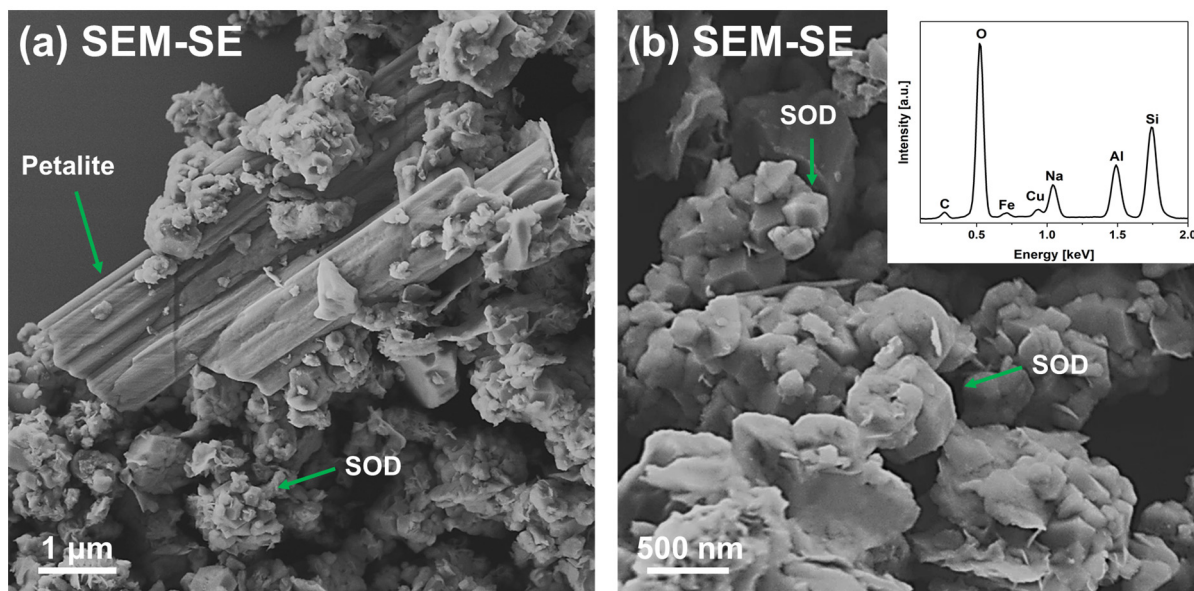


Figure 7. SEM-SE images of leaching residues obtained under optimal conditions show (a) an unreacted petalite fragment within hydrosodalite crystals and (b) intergrown isometric hydrosodalite crystals exhibiting a distinct dodecahedral habit, being mainly composed of Na, Al, Si, and O (SEM-EDS), while small Cu signals originate from sample coating.

BET measurements were performed on both petalite starting material and samples milled in 7 mol/L NaOH for different times, corresponding to Figure 5 (PXRD) and Figure 6

(FTIR). As expected, the starting material displayed a low BET surface area of 1 m²/g, while significantly higher values of 10, 12, and 19 m²/g were obtained with increasing time after 30, 60, and 120 min of ball milling, respectively. An explanation for the increase in N₂ adsorption capacity for the 30 and 60 min samples is related to the reduction in the particle size associated with an increase in surface area, while conversion to a more porous zeolite framework additionally contributed, which is particularly evident for the 120 min sample.

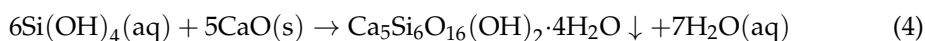
Reference experiments involving ball milling in water and regular leaching were conducted on petalite samples to determine crystallite size without chemical side reactions and to address the question of whether the use of ball milling is essential for lithium leaching and/or zeolite formation. In this context, PXRD measurements on samples milled just in water revealed a broadening of the diffraction peaks which were used to determine the crystallite size (*D*) according to Scherrer's equation (Equation (3)), where *K* represents the Scherrer constant, λ the wavelength of the radiation, *B* the full width at half maximum (FWHM) intensity, and Θ the Bragg angle.

$$D = K * \lambda / (B * \cos \theta) \quad (3)$$

Calculations using the main diffraction peak at 27.765° assumed *K* = 0.9 (according to Salakjani et al. [33]) to reveal a reduction in crystallite size to 1620 and 1480 Å (compared to a starting value of approximately 500 μm) after milling for 60 or 120 min, respectively. At the same time, ICP-OES measurements on water samples indicate a slight loss of lithium of up to 143 mg/L, corresponding to an extraction of about 5.9%. The regular leaching experiments without intensive milling were performed under parameters as for the mechanochemical trials, maintaining the concentration of NaOH, time, temperature, and LSR at 7 mol/L, 120 min, 90 °C, and 10:1 mL/g, respectively, while the suspension was stirred at 500 rpm. As expected, the extraction yield was much lower, reaching only 3.4%, while PXRD data of the leaching residues confirmed this trend by revealing no significant changes in the diffraction pattern. Hence, as a result of the reference experiments, it can be concluded that the ball milling process and the associated mechanical activation, including the formation of new reactive surfaces, enables the effective reaction with the caustic soda, which is apparently essential for effective lithium extraction in parallel with zeolite formation.

Desilication became mandatory as an intermediate step due to the rather high silicon content of 38.4 g/L in the petalite leachate, which generally facilitates the formation of by-products during further processing. Considering that the desilication of similar solutions using CaO had already been investigated by several authors [21,29], only different CaO:SiO₂ ratios between 0.6 and 1.4 were tested in this study while the temperature and stirring speed were kept constant. Experimental results (see Figure 8) show that most of the Si was successfully removed after 30 min while a longer reaction time leads only to a slight increase in yield, reaching a plateau at about 60 min.

In terms of CaO consumption and removal efficiency, a CaO:SiO₂ ratio of 0.8 is preferred, with 94.6% of the Si removed after a period of no more than 60 min while a slightly higher value of 95.1% was reached after 90 min time. In addition, ICP-OES measurements of the solution after desilication revealed elemental concentrations of Al (0.1 g/L), Li (2.7 g/L), and Si (1.9 g/L), indicating constant lithium content, while significantly lower values were obtained for Al and especially Si. In addition to analysis of the solution, PXRD studies of the precipitates (see Figure 9) revealed torbermorite (Ca₅Si₆O₁₆(OH)₂·4H₂O; PDF#98-008-7690) as the main phase after desilication, which forms according to Equation (4) and transforms into wollastonite (Ca[SiO₃]; PDF#98-020-1537) following Equation (5) when calcined at 900 °C for at least 30 min. Wollastonite, in particular, is an advantageous by-product since it offers numerous technical applications due to its high melting point and fibrous to acicular structure, thus providing an additional benefit for the entire route [34].



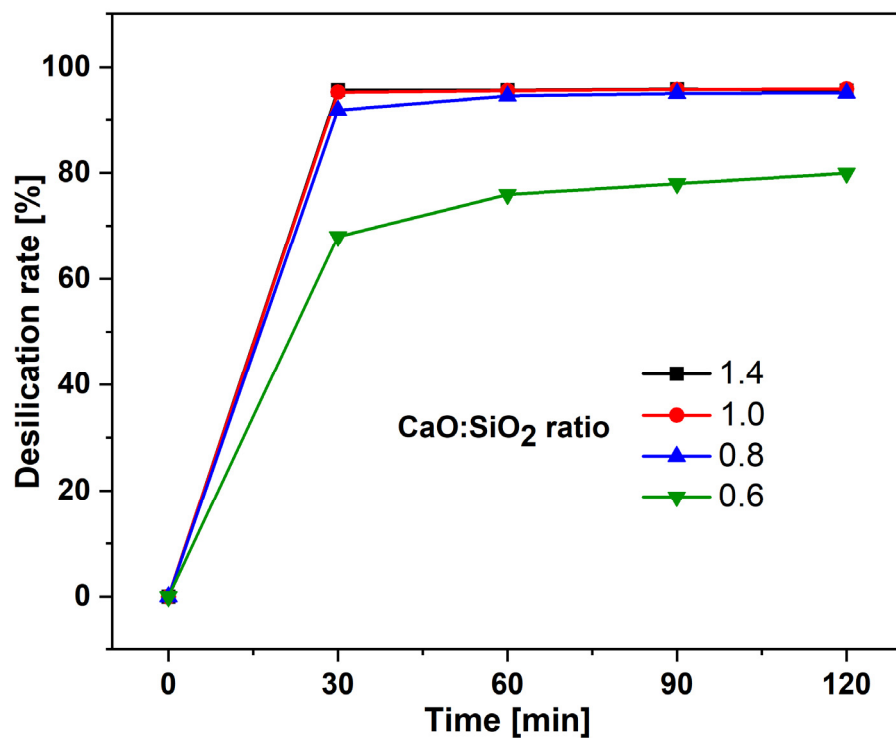


Figure 8. Desiccation of the leaching solution as a function of different reaction time using different mass ratios of CaO:SiO₂.

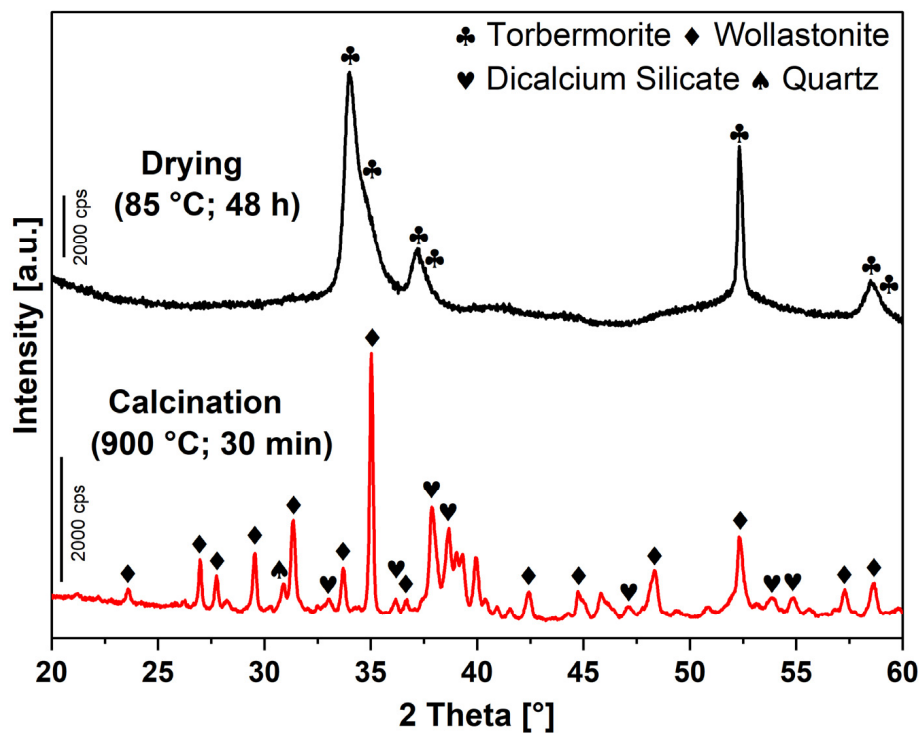


Figure 9. PXRD patterns desiccation by-products obtained after drying at 85 °C for 48 h and after calcination at 900 °C for 30 min.

Precipitation of the dissolved lithium (approx. 3.0 g/L) as an easily handled compound can be considered as one of the key factors of the whole process. Since the lithium content in solution was too low for precipitation of Li_2CO_3 , it requires contents of 10 g/L or more; the phosphoric acid approach [23] was chosen to precipitate Li_3PO_4 following Equation (6), which has a remarkably low solubility of 0.38 g/L at 20 °C in comparison to the well dissolvable sodium phosphate Na_3PO_4 (121 g/L at 20 °C).



Therefore, H_3PO_4 was added to the leachate at a temperature of 90 °C and at different P:Li ratios ranging between 1.0:3.0 and 1.8:3.0 to examine the influence of this parameter on the lithium recovery and the composition of the obtained products shown in Table 2. The recovery increased significantly with higher amounts of phosphoric acid and reached its maximum at the ratio 1.8:3.0 with 91.1%.

Table 2. Lithium recovery and obtained products using different P:Li ratios.

P:Li Ratio	Li Recovery (%)	Product
1.8:3.0	91.1	Li_3PO_4 ; Li_2NaPO_4
1.6:3.0	86.9	Li_3PO_4 ; Li_2NaPO_4
1.4:3.0	81.2	Li_3PO_4 ; Li_2NaPO_4
1.2:3.0	72.9	Li_3PO_4
1.0:3.0	76.7	Li_3PO_4 ; Li_2NaPO_4

However, at higher P:Li ratios, mixed phosphates with orthorhombic nalipoite structure (Li_2NaPO_4) were formed in addition to Li_3PO_4 , as confirmed by PXRD (see Figure 10). Since the purity of the precipitate is of great importance for further applications, a P:Li ratio of 1.2:3.0 is clearly preferred despite the comparatively low recovery of 72.9%, since here, pure Li_3PO_4 was detected in the corresponding diffraction patterns.

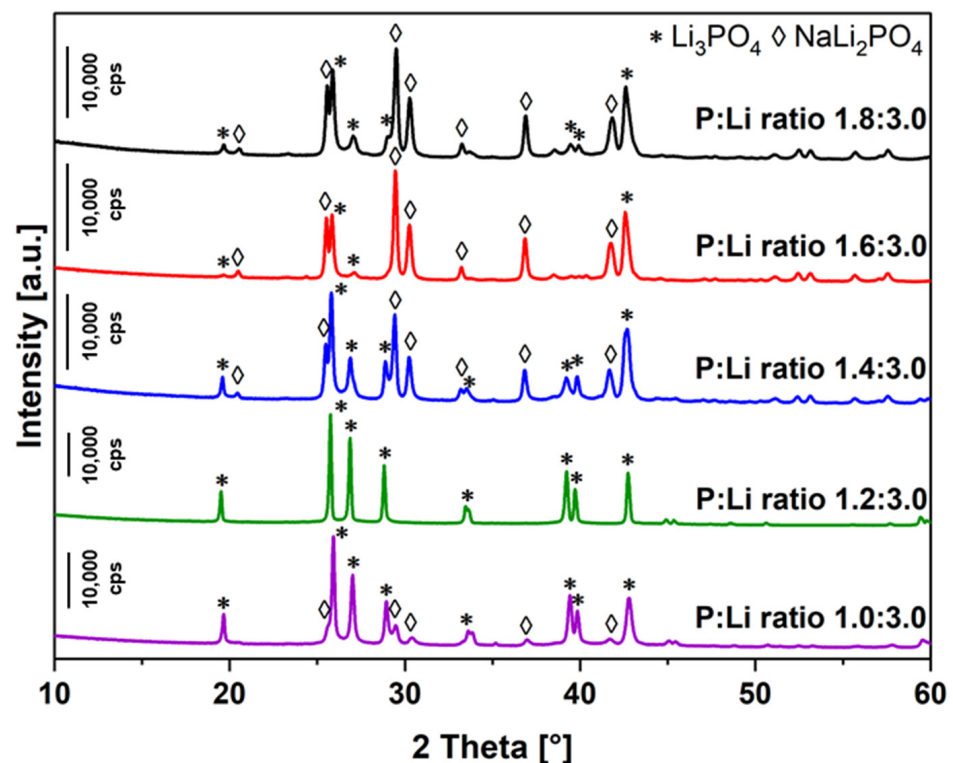
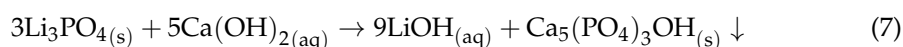


Figure 10. PXRD pattern of different phosphates after precipitation using different P:Li ratios.

It should be mentioned that the absolute yield is not that important since the spent liquor still has a high pH, which potentially allows reuse in another extraction process after adding fresh NaOH, with the added benefit that unprecipitated lithium remains in circulation. However, the formation of mixed Na–Li phosphates, especially at higher P:Li ratios, has already been mentioned by several authors and is generally a challenge due to the low lithium–sodium ratio in the liquor [20,23,29]. In addition, it is worth mentioning that the optimal ratios at which pure Li_3PO_4 could be obtained vary slightly between authors, from 1.2:3.0 to 1.6:3.0, which may be due to different Na:Li ratios in the different approaches [20,23,29].

In general, lithium phosphate is versatile as a precursor for the synthesis of Li–Fe phosphate cathode materials or lithium-based compounds such as carbonates or hydroxides, which are currently in high demand [23,35,36]. In the following section, the conversion of lithium phosphate to lithium hydroxide is shown using calcium hydroxide, which acts as a phosphate collector in accordance with Equation (7).



To confirm this reaction, PXRD measurements were chosen to reveal the presence of hydroxylapatite ($\text{Ca}_5(\text{PO}_4)_3\text{OH}$, PDF#98-008-1442) besides non-converted $\text{Ca}(\text{OH})_2$ (PDF#98-007-3467) in the precipitates (see Figure 11), while lithium hydroxide initially remained in solution and may be obtained after crystallization in the form of $\text{LiOH}\cdot\text{H}_2\text{O}$ (PDF# 98-003-5155).

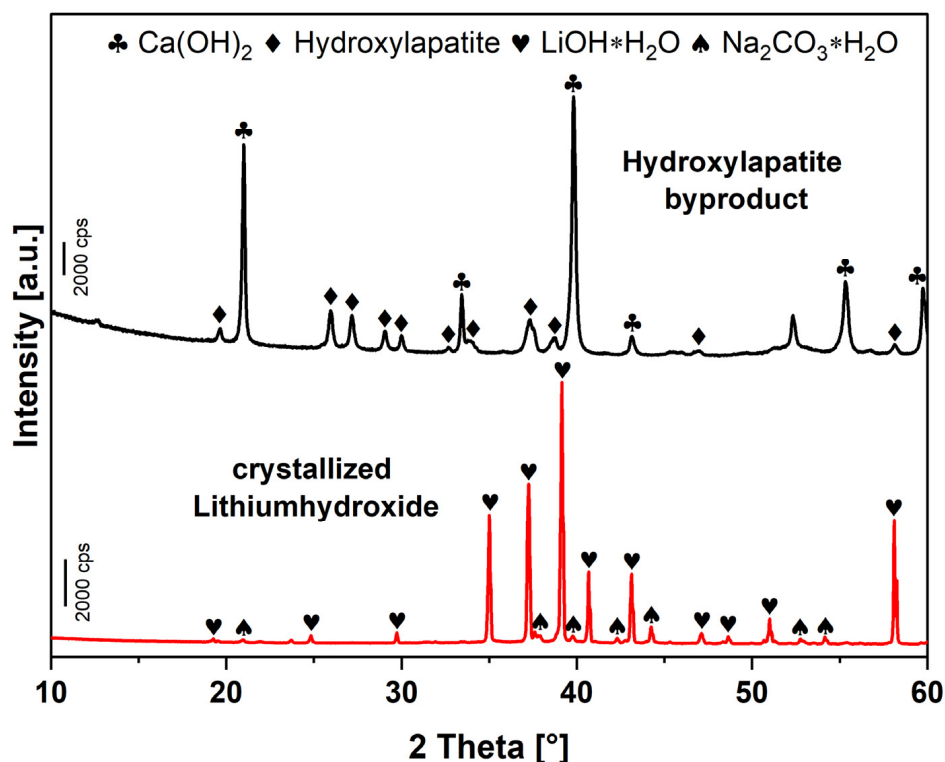


Figure 11. PXRD patterns of hydroxylapatite by-product and lithium hydroxide obtained after complete crystallization of the solution.

Since apatite is one of the most commonly used P sources for fertilizers [37], it can be considered as a value-added by-product within this process. When assessing the purity of the hydroxide, PXRD showed traces of $\text{Na}_2\text{CO}_3\cdot\text{H}_2\text{O}$ (PDF#98-000-6293) while ICP-OES indicated minor impurities of Na and Ca, resulting in an overall purity of 99%, since C is not detectable by this method. In particular, because of its high affinity for CO_2 , crystallization

in an inert atmosphere is essential to avoid the formation of Li_2CO_3 during this final precipitation step.

Adsorption experiments on synthetic wastewater samples containing heavy metal ions were adopted to investigate the sorption behavior of the synthesized zeolite by-product. Therefore, a removal efficiency was calculated for each experiment based on ICP-OES results and plotted in Figure 12 as a function of zeolite dosage.

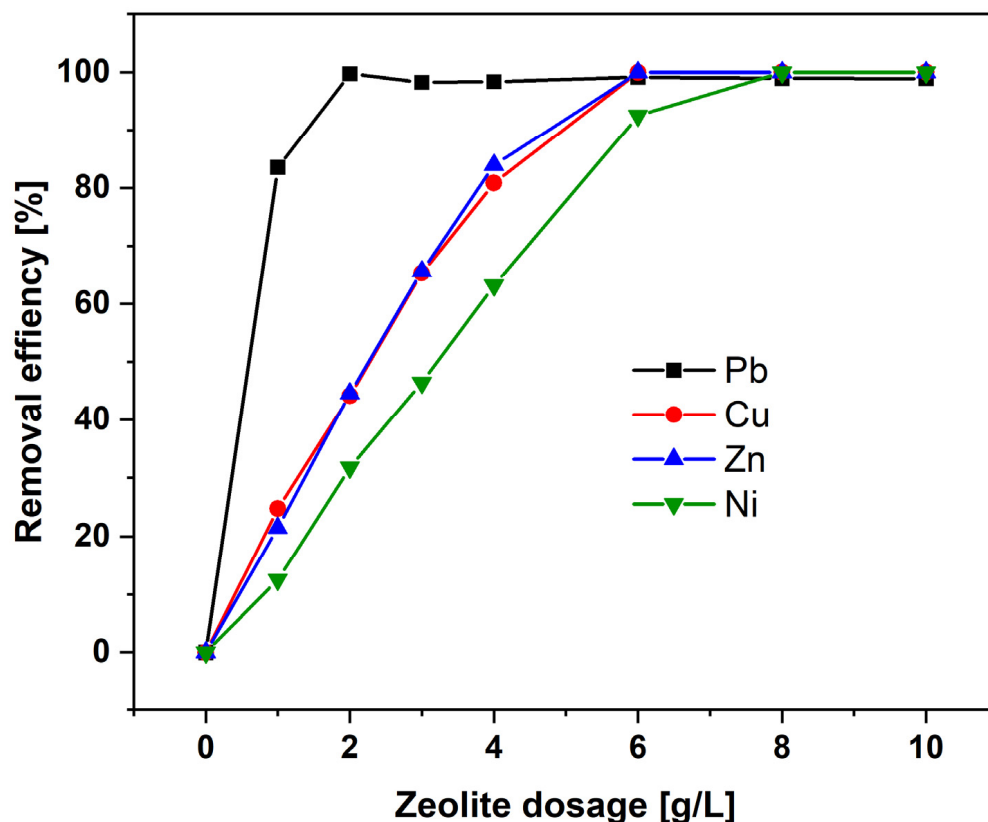


Figure 12. Removal efficiency (%) for divalent heavy metal ions of Pb, Cu, Zn, and Ni in synthetic wastewater solutions as a function of zeolite dosage (g/L).

The removal efficiency for all metal ions significantly increased with rising zeolite dosage, as expected. Here, the excellent sorption of Pb^{2+} is most noticeable as 99.7% was adsorbed already at 2 g/L whereas a nearly complete adsorption of Cu^{2+} , Zn^{2+} , and Ni^{2+} requires higher dosages of at least 6 or 8 g/L, respectively. Comparing the obtained results (see Table 3) with similar studies of He et al. [38], Esaifan et al. [26], and Necke et al. [29] using hydrosodalites or related zeolites at the same dosage of 6 g/L, it is observed that the sorption of Cu^{2+} and Pb^{2+} is generally preferred, reaching removal efficiencies between 90 and 100%.

Table 3. Removal efficiencies [%] for divalent heavy metal ions in synthetic wastewater solutions at a zeolite dosage of 6 g/L.

[%]	This Work	Necke et al. [29]	Esaifan et al. [26]	He et al. [38]
Pb^{2+}	99	99	99	100
Cu^{2+}	100	100	90	95
Ni^{2+}	92	100	54	65
Zn^{2+}	100	86	62	-

An explanation for the rather high sorption of Pb and Cu can be rationalized by different ionic radii which significantly control the mobility of the heavy metal ions

within zeolite pores and channels. Therefore, sorption would be expected in the order $\text{Pb}^{2+} > \text{Ni}^{2+} > \text{Cu}^{2+} > \text{Zn}^{2+}$ corresponding to hydrated ionic radii of 4.01, 4.04, 4.19, and 4.3 Å [26,38,39], respectively, which is consistent with the experimental results for Pb and Cu. In the case of Ni, ionic radii may also play a role but here the initial pH of the water is of considerable importance, as reported by He et al. [38] who studied the sorption behavior at different pH values. Therefore, the high sorption of nickel in this work (92%) and our earlier study (100%) may be related to the slightly higher pH of 5.8 which is quite close to the full adsorption potential of nickel at pH 6 [38]. Besides the ionic radii and the initial pH of the solution, it can be assumed that the different synthesis routes for hydrosodalites, e.g., hydrothermal vs. mechanochemical as well as the different starting materials such as fly ash [38], low-grade kaolin [26], LAS glass-ceramics [29], or petalite (this study) can influence the resulting sorption behavior due to differences for instance in particle size and/or specific surface. In conclusion, this type of adsorption is clearly the result of a cation exchange (e.g., Pb^{2+} vs. 2Na^+) within the zeolite structure which is possible since the hydrated radius of Na^+ (5.6 Å) [40] and its charge are similar to the heavy metal ions studied here.

4. Discussion

When comparing the ICP-OES and the PXRD data, a clear trend becomes visible, indicating that effective lithium extraction only takes place if it is possible to decompose the parent phase by intense mechanical and/or chemical forces. An explanation of a much higher leachability and reactivity of petalite compared to spodumene or lepidolite during the experimental investigations can be given by a closer look at the crystallographic features. Comparing the crystal structure at the unit cell level (see Figure 13), it is obvious that petalite is generally less densely packed than lepidolite and α -spodumene, having a more open three-dimensional network structure which is generally advantageous for the leaching process.

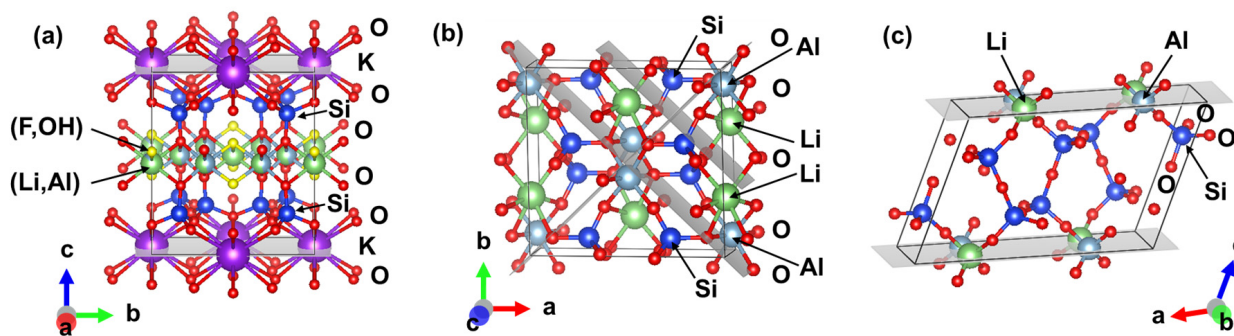


Figure 13. Idealized crystal structures on the unit cell level of the investigated minerals (a) lepidolite, (b) spodumene, and (c) petalite. The grayish colored areas indicate the most important cleavage planes within the structures while the orientation of the unit cell is given next to each structure. Notably, the figures were created using VESTA 3 employing atomic radii [41].

Moreover, apart from the lower packing density of petalite, Li^+ and Al^{3+} reveal a tetrahedral rather than octahedral coordination in addition to a lower refractive index and a lower birefringence when petalite is compared to lepidolite or spodumene (see Table 4) [42,43]. In addition, atomic packing calculations by Welsch et al. [44] gave an ionic porosity of $Z \approx 43.5$ for α -spodumene; whereas, studies on petalite samples resulting in a much higher value of $Z \approx 57.8$ suggest a much more open crystal structure which is in general favorable for lithium leaching. Indeed, evidence for higher lithium mobility in petalite could be given by Effenberger et al. who replaced lithium against hydrogen using concentrated H_2SO_4 at 300 °C for 90 h to prepare Li/H-exchanged petalite ($\text{HAlSi}_4\text{O}_{10}$) for structural investigations [45].

In addition to packing and bonding within the unit cell, the activation of specific cleavage planes within the silicate minerals by intensive ball milling is considered to be a crucial factor for lithium release during mechanochemical treatment.

Table 4. Selected physical and optical properties of investigated minerals [46–48].

	Lepidolite	Spodumene	Petalite
Density [g/cm ³]	2.84	3.18	2.4
Refractive Indices n_α	1.530	1.648–1.661	1.504
Refractive Indices n_β	1.551–1.556	1.655–1.670	1.510
Refractive Indices n_γ	1.555–1.559	1.662–1.679	1.516
Birefringence δ	0.025–1.559	0.014–0.018	0.012
Coordination of Li	6	6	4

In lepidolite (see Figure 13a), a typically layered phyllosilicate, the relatively strong bonding forces of Si–O and Al–O within the tetrahedral layer and the tight bonding to the octahedral layer are responsible for the perfect cleavage between the layer packets along (001), where the relatively large K⁺ cations are located for charge balance while Li⁺ is bound to the octahedral layer replacing part of the Al³⁺ [49]. In consequence, mechanochemical treatment of the lepidolite samples results in cleavage along the 001 plane, preferentially leaching K⁺, while Li⁺ remained trapped in the octahedral layer, resulting in an extraction rate of 32.0% for K while at the same time only 18.2% of Li was extracted.

In contrast, the crystal structure of the inosilicate spodumene (see Figure 13b) consists of parallel chains of [SiO₄]-tetrahedra and [AlO₆]-octahedra which both run in the direction of the c-axis and are connected by corners while Li⁺ cations fill gaps within the structure [49]. Spodumene exhibits perfect cleavages along the (110) and (1-10) directions and intersects at an angle of 87° which is a characteristic feature of the entire pyroxene group [49]. Ball milling of spodumene is expected to lead to the activation of both cleavage systems, resulting in the breaking of several bonds which only slightly increases the leachability of lithium. However, since lithium has a 6-fold coordination in spodumene, this effect is negligible which can be confirmed by the experimental results indicating a low extraction rate of 28.4% for lithium even under the most intense conditions.

The crystal structure of petalite (see Figure 13c) consists of a three-dimensional arrangement of TO₄ tetrahedra (with T = Li; Al or Si) connected by corners sharing one oxygen [50]. Due to the perfect arrangement of cations on certain crystallographic planes, petalite can also be considered as a phyllosilicate built up of folded [Si₄O₁₀] layers perpendicular to (001) connected by LiO₄ and AlO₄ tetrahedra [50]. Particularly noteworthy is the tetrahedral coordination of Al³⁺ and Li⁺ [43] which distinguishes petalite from lepidolite and spodumene. The perfect cleavage of petalite runs exactly parallel to these sheets and perpendicular to (001) where the weakest bonds in the structure are expected to be present. During the mechanochemical treatment, petalite crystals are preferentially cleaved along this direction, leading to new surfaces containing Li sites, which, in addition to the more open petalite framework and the lower coordination of Li, are essential for successful lithium extraction, reaching 84.9% under optimum conditions.

The overall results for the processing of petalite in the context of mechanochemical lithium extraction are summarized in a flow chart (see Figure 14) containing both the optimum experimental parameters and the yields achieved.

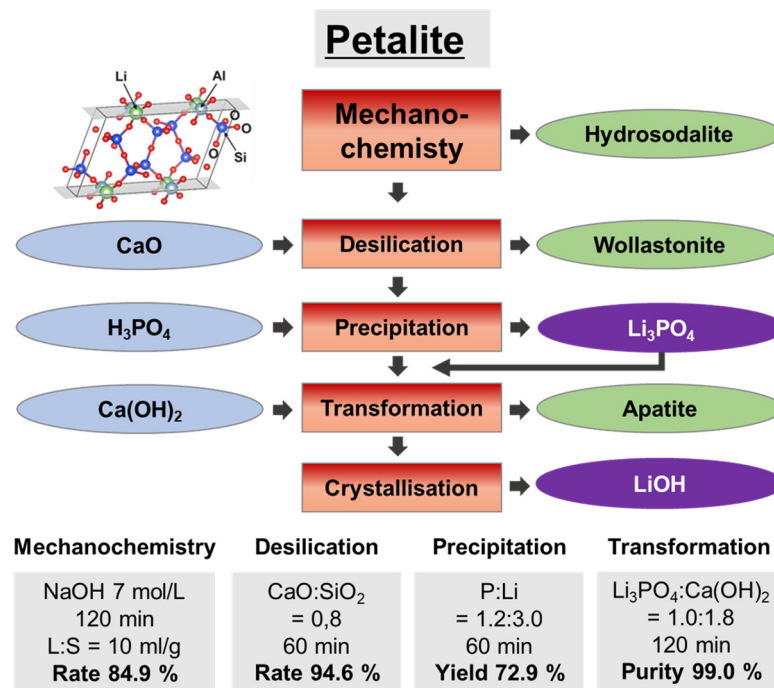


Figure 14. Flowchart of the mechanochemical extraction of lithium from petalite.

5. Conclusions

In this work, we investigated the transferability of our previously established mechanochemical route for lithium extraction to the three most common lithium silicate minerals: lepidolite, spodumene, and petalite. The insights gained from these investigations were as follows.

Experimental results show that petalite is much more suitable for the alkaline mechanochemical approach than spodumene or lepidolite, resulting in a substantial lithium extraction of 84.9% and almost complete conversion to hydrosodalite after 120 min of ball milling in alkaline media. An explanation for the higher reactivity under these circumstances is related to special features of the petalite crystal structure which include less dense packing and the activation of cleavage planes along lithium sites during ball milling.

After mechanochemical leaching of petalite, 60 min of desilication of the caustic solution at a CaO:SiO₂ ratio of 0.8 already resulted in a silica removal of 94.6%, whereas, the lithium content was not affected. In addition, wollastonite was recovered as a value-added by-product by this intermediate step. Subsequently, lithium was precipitated as pure Li₃PO₄ by adding H₃PO₄ in a P:Li ratio of 1.2:3.0 where a yield of 72.9% was achieved. Finally, the conversion of Li₃PO₄ to LiOH·H₂O with a high purity of 99% was demonstrated using Ca(OH)₂.

Hydrosodalites obtained as a by-product of petalite leaching exhibit a relatively high specific surface area up to 18.5 m²/g and excellent sorption efficiency for Cu²⁺ (100%), Zn²⁺ (100%), Pb²⁺ (99.1%), and Ni²⁺ (92.5%) at a dosage of 6 g/L when used to treat synthetic wastewater samples.

The results obtained during this study encourage the authors to extend the described mechanochemical route for the recovery of lithium from end-of-life batteries in the future.

Author Contributions: Conceptualization, T.N. and H.-J.K.; methodology, T.N.; validation, T.N. and H.-J.K.; formal analysis, T.N. and J.S.; investigation, T.N. and J.S.; resources, H.-J.K. and B.B.-G.; writing—original draft preparation, T.N., J.S., H.-J.K. and B.B.-G.; writing—review and editing, T.N., J.S., H.-J.K. and B.B.-G.; visualization, T.N. and J.S.; supervision, H.-J.K. and B.B.-G.; project administration, T.N., H.-J.K. and B.B.-G.; funding acquisition, B.B.-G. All authors have read and agreed to the published version of the manuscript.

Funding: This research received no external funding.

Data Availability Statement: The data presented in this study are available on request from the corresponding author.

Acknowledgments: The authors would like to thank Nina Kintop, Regine Peter, Jürgen Dieter Rossa and Birgit Huth for their assistance with ICP-OES, BET, SEM, and LOI analysis, respectively. We also thank Katrin Berberich for the intensive discussion of the experimental results, Christian Bracke for providing the lepidolite sample, and Svenja Schroeder for performing the reference experiments.

Conflicts of Interest: The authors declare no conflict of interest. The funders had no role in the design of the study; in the collection, analyses, or interpretation of data; in the writing of the manuscript; or in the decision to publish the results.

References

1. Swain, B. Recovery and recycling of lithium: A review. *Sep. Purif. Technol.* **2017**, *172*, 388–403. [\[CrossRef\]](#)
2. Deberitz, J.; Boche, G. Lithium und seine Verbindungen-Industrielle, medizinische und wissenschaftliche Bedeutung. *Chem. Unserer Zeit* **2003**, *37*, 258–266. [\[CrossRef\]](#)
3. Schmidt, M. *Rohstoffrisikobewertung Lithium*; Bundesanstalt für Geowissenschaften und Rohstoffe (BGR), Deutsche Rohstoffagentur (DERA): Berlin, Germany, 2017.
4. U.S. Geological Survey. *Mineral Commodity Summaries 2023*; U.S. Geological Survey: Reston, VA, USA, 2023; ISBN 978-1-4113-4504-1.
5. Holleman, A.F.; Wiberg, E.; Wiberg, N. *Grundlagen und Hauptgruppenelemente: Band 1: Grundlagen und Hauptgruppenelemente*, 103rd ed.; De Gruyter: Berlin, Germany, 2016; ISBN 978-3-11-049585-0.
6. Garrett, D.E. *Handbook of Lithium and Natural Calcium Chloride*; Elsevier: Amsterdam, The Netherlands, 2004; ISBN 0080472907.
7. Meshram, P.; Pandey, B.D.; Mankhand, T.R. Extraction of lithium from primary and secondary sources by pre-treatment, leaching and separation: A comprehensive review. *Hydrometallurgy* **2014**, *150*, 192–208. [\[CrossRef\]](#)
8. Kesler, S.E.; Gruber, P.W.; Medina, P.A.; Keoleian, G.A.; Everson, M.P.; Wallington, T.J. Global lithium resources: Relative importance of pegmatite, brine and other deposits. *Ore Geol. Rev.* **2012**, *48*, 55–69. [\[CrossRef\]](#)
9. Li, H.; Eksteen, J.; Kuang, G. Recovery of lithium from mineral resources: State-of-the-art and perspectives—A review. *Hydrometallurgy* **2019**, *189*, 105129. [\[CrossRef\]](#)
10. Vikström, H.; Davidsson, S.; Höök, M. Lithium availability and future production outlooks. *Appl. Energy* **2013**, *110*, 252–266. [\[CrossRef\]](#)
11. Vieceli, N.; Nogueira, C.A.; Pereira, M.F.; Dias, A.P.S.; Durão, F.O.; Guimarães, C.; Margarido, F. Effects of mechanical activation on lithium extraction from a lepidolite ore concentrate. *Miner. Eng.* **2017**, *102*, 1–14. [\[CrossRef\]](#)
12. Salakjani, N.K.; Singh, P.; Nikoloski, A.N. Production of Lithium—A Literature Review Part 1: Pretreatment of Spodumene. *Miner. Process. Extr. Metall. Rev.* **2020**, *41*, 335–348. [\[CrossRef\]](#)
13. Sitando, O.; Crouse, P.L. Processing of a Zimbabwean petalite to obtain lithium carbonate. *Int. J. Miner. Process.* **2012**, *102–103*, 45–50. [\[CrossRef\]](#)
14. Tadesse, B.; Makuei, F.; Albijanic, B.; Dyer, L. The beneficiation of lithium minerals from hard rock ores: A review. *Miner. Eng.* **2019**, *131*, 170–184. [\[CrossRef\]](#)
15. Peltosaari, O.; Tanskanen, P.; Heikkinen, E.-P.; Fabritius, T. $\alpha \rightarrow \gamma \rightarrow \beta$ -phase transformation of spodumene with hybrid microwave and conventional furnaces. *Miner. Eng.* **2015**, *82*, 54–60. [\[CrossRef\]](#)
16. Gasalla, H.J.; Aglietti, E.F.; Lopez, J.; Pereira, E. Changes in physicochemical properties of α -spodumene by mechanochemical treatment. *Mater. Chem. Phys.* **1987**, *17*, 379–389. [\[CrossRef\]](#)
17. Kotsupalo, N.P.; Menzheres, L.T.; Ryabtsev, A.D.; Boldyrev, V.V. Mechanical activation of α -spodumene for further processing into lithium compounds. *Theor. Found. Chem. Eng.* **2010**, *44*, 503–507. [\[CrossRef\]](#)
18. Vieceli, N.; Nogueira, C.A.; Pereira, M.F.C.; Durão, F.O.; Guimarães, C.; Margarido, F. Optimization of an innovative approach involving mechanical activation and acid digestion for the extraction of lithium from lepidolite. *Int. J. Min. Met. Mater.* **2018**, *25*, 11–19. [\[CrossRef\]](#)
19. Han, G.; Gu, D.; Lin, G.; Cui, Q.; Wang, H. Recovery of lithium from a synthetic solution using spodumene leach residue. *Hydrometallurgy* **2018**, *177*, 109–115. [\[CrossRef\]](#)
20. Lv, Y.; Xing, P.; Ma, B.; Liu, Y.; Wang, C.; Zhang, W.; Chen, Y. Efficient Extraction of Lithium and Rubidium from Polyolithionite via Alkaline Leaching Combined with Solvent Extraction and Precipitation. *ACS Sustain. Chem. Eng.* **2020**, *8*, 14462–14470. [\[CrossRef\]](#)
21. Xing, P.; Wang, C.; Zeng, L.; Ma, B.; Wang, L.; Chen, Y.; Yang, C. Lithium Extraction and Hydroxysodalite Zeolite Synthesis by Hydrothermal Conversion of α -Spodumene. *ACS Sustain. Chem. Eng.* **2019**, *7*, 9498–9505. [\[CrossRef\]](#)
22. Ivanenko, O.; Pavlenko, T. Hydrothermal Extraction of Lithium Compounds from Petalite $\text{Li}[\text{AlSi}_4\text{O}_{10}]$. *Ukr. Chem. J.* **2021**, *87*, 45–54. [\[CrossRef\]](#)

23. Mulwanda, J.; Senanayake, G.; Oskierski, H.; Altarawneh, M.; Dlugogorski, B.Z. Leaching of lepidolite and recovery of lithium hydroxide from purified alkaline pressure leach liquor by phosphate precipitation and lime addition. *Hydrometallurgy* **2021**, *201*, 105538. [CrossRef]
24. Song, Y.; Zhao, T.; He, L.; Zhao, Z.; Liu, X. A promising approach for directly extracting lithium from α -spodumene by alkaline digestion and precipitation as phosphate. *Hydrometallurgy* **2019**, *189*, 105141. [CrossRef]
25. Qiu, S.; Zhu, Y.; Jiang, Y.; Liu, C.; Yu, J. Kinetics and Mechanism of Lithium Extraction from α -Spodumene in Potassium Hydroxide Solution. *Ind. Eng. Chem. Res.* **2022**, *61*, 15103–15113. [CrossRef]
26. Esaifan, M.; Warr, L.N.; Grathoff, G.; Meyer, T.; Schafmeister, M.-T.; Kruth, A.; Testrich, H. Synthesis of Hydroxy-Sodalite/Cancrinite Zeolites from Calcite-Bearing Kaolin for the Removal of Heavy Metal Ions in Aqueous Media. *Minerals* **2019**, *9*, 484. [CrossRef]
27. Nabavi, M.S.; Mohammadi, T.; Kazemimoghadam, M. Hydrothermal synthesis of hydroxy sodalite zeolite membrane: Separation of H₂/CH₄. *Ceram. Int.* **2014**, *40*, 5889–5896. [CrossRef]
28. Khajavi, S.; Jansen, J.C.; Kapteijn, F. Production of ultra pure water by desalination of seawater using a hydroxy sodalite membrane. *J. Membr. Sci.* **2010**, *356*, 52–57. [CrossRef]
29. Necke, T.; Wolf, D.M.; Bachmann, A.-L.; Berberich, K.; Kleebe, H.-J.; Weidenkaff, A. Mechanochemical Lithium Extraction and Zeolite Synthesis from End-of-Life Glass–Ceramics. *ACS Sustain. Chem. Eng.* **2022**, *10*, 10849–10857. [CrossRef]
30. Xing, P.; Wang, C.; Wang, L.; Ma, B.; Chen, Y.; Wang, G. Clean and efficient process for the extraction of rubidium from granitic rubidium ore. *J. Clean. Prod.* **2018**, *196*, 64–73. [CrossRef]
31. Tagai, T.; Ried, H.; Joswig, W.; Korekawa, M. Kristallographische Untersuchungen eines Petalits mittels Neutronenbeugung und Transmissionselektronenmikroskopie. *Z. Krist.* **1982**, *160*, 159–170. [CrossRef]
32. Marsh, A.; Heath, A.; Patureau, P.; Evernden, M.; Walker, P. A mild conditions synthesis route to produce hydrosodalite from kaolinite, compatible with extrusion processing. *Microporous Mesoporous Mater.* **2018**, *264*, 125–132. [CrossRef]
33. Salakjani, N.K.; Singh, P.; Nikoloski, A.N. Mineralogical transformations of spodumene concentrate from Greenbushes, Western Australia. Part 1: Conventional heating. *Miner. Eng.* **2016**, *98*, 71–79. [CrossRef]
34. Ismail, H.; Shamsudin, R.; Abdul Hamid, M.A. Effect of autoclaving and sintering on the formation of β -wollastonite. *Mater. Sci. Eng. C Mater. Biol. Appl.* **2016**, *58*, 1077–1081. [CrossRef]
35. Franger, S.; Le Cras, F.; Bourbon, C.; Rouault, H. LiFePO₄ Synthesis Routes for Enhanced Electrochemical Performance. *Electrochem. Solid-State Lett.* **2002**, *5*, A231. [CrossRef]
36. Maccario, M.; Croguennec, L.; Wattiaux, A.; Suard, E.; Lecras, F.; Delmas, C. C-containing LiFePO₄ materials—Part I: Mechanochemical synthesis and structural characterization. *Solid State Ion.* **2008**, *179*, 2020–2026. [CrossRef]
37. Hughes, J.M. The many facets of apatite. *Am. Mineral.* **2015**, *100*, 1033–1039. [CrossRef]
38. He, K.; Chen, Y.; Tang, Z.; Hu, Y. Removal of heavy metal ions from aqueous solution by zeolite synthesized from fly ash. *Environ. Sci. Pollut. Res. Int.* **2016**, *23*, 2778–2788. [CrossRef]
39. Golomeova, M.; Zendelska, A.; Blazev, K.; Krstev, B.; Golomeov, B. Removal of Heavy Metals from Aqueous Solution using Clinoptilolite and Stilbite. *Int. J. Eng. Res. Technol.* **2014**, *3*, 1029–1035.
40. Hannachi, C.; Ali, M.B.S.; Hamrouni, B. Determination of the selectivity coefficient of the CMX cationic membrane at various ionic strengths. *Desalination Water Treat.* **2009**, *10*, 47–52. [CrossRef]
41. Momma, K.; Izumi, F. VESTA 3 for three-dimensional visualization of crystal, volumetric and morphology data. *J. Appl. Crystallogr.* **2011**, *44*, 1272–1276. [CrossRef]
42. Černý, P.; London, D. Crystal chemistry and stability of petalite. *TMPM Tschermaks Petr. Mitt.* **1983**, *31*, 81–96. [CrossRef]
43. Zemmann-Hedlik, A.; Zemmann, J. Die Kristallstruktur von Petalit, LiAlSi₄O₁₀. *Acta Cryst.* **1955**, *8*, 781–787. [CrossRef]
44. Welsch, A.-M.; Behrens, H.; Ross, S.; Murawski, D. Structural control of ionic conductivity in LiAlSi₂O₆ and LiAlSi₄O₁₀ glasses and single crystals. *Z. Phys. Chem.* **2012**, *226*, 491–511. [CrossRef]
45. Effenberger, H.; Fuess, H.; Müller, G.; Vogt, T. Crystal structure and hydrogen bonding in Li/H-exchanged petalite, HAlSi₄O₁₀. *Z. Krist.* **1991**, *197*, 27–40. [CrossRef]
46. mindat.org. Lepidolite-Entry in the Database. Available online: <https://www.mindat.org/min-2380.html> (accessed on 26 June 2023).
47. mindat.org. Spodumene-Entry in the Database. Available online: <https://www.mindat.org/min-3733.html> (accessed on 26 June 2023).
48. mindat.org. Petalite-Entry in the Database. Available online: <https://www.mindat.org/min-3171.html> (accessed on 26 June 2023).
49. Okrusch, M.; Matthes, S. *Mineralogie: Eine Einführung in Die Spezielle Mineralogie, Petrologie und Lagerstättenkunde*, 9th ed.; Springer Gabler: Wiesbaden, Germany, 2014; ISBN 978-3-64-234659-0.
50. Haussühl, E.; Schreuer, J.; Winkler, B.; Haussühl, S.; Bayarjargal, L.; Milman, V. Structure-property relations and thermodynamic properties of monoclinic petalite, LiAlSi₄O₁₀. *J. Phys. Condens. Matter* **2012**, *24*, 345402. [CrossRef] [PubMed]

Disclaimer/Publisher's Note: The statements, opinions and data contained in all publications are solely those of the individual author(s) and contributor(s) and not of MDPI and/or the editor(s). MDPI and/or the editor(s) disclaim responsibility for any injury to people or property resulting from any ideas, methods, instructions or products referred to in the content.